Nematic liquid crystal disclination lines driven by a photo-aligned defect grid

*Inge Nys, Brecht Berteloot, Jeroen Beeckman, and Kristiaan Neyts**

I. Nys, B. Berteloot, J. Beeckman, K. Neyts,
Liquid Crystals & Photonics Group, Department of Electronics and Information Systems,
Ghent University, Technologiepark-Zwijnaarde 126, 9052 Ghent, Belgium
E-mail: Kristiaan.Neyts@Ugent.be

Keywords: disclination lines, defect grids, photo-alignment, nematic liquid crystals

Photo-alignment for nematic liquid crystals makes it possible to design complex alignment patterns with point defects, that can act as anchoring points for disclination lines. This feature may be used to realize novel electro-optical devices with bistability or enhanced scattering and is promising for material applications such as stimuli-responsive actuators, active matter and assembly of colloidal particles. However, the applicability is hampered by the limited understanding of the interaction between the defects in the photo-alignment pattern and the disclination lines in the nematic liquid crystal. In this work we study disclination lines that connect surface defects of strength 1/2 arranged in a periodic grid. We estimate the elastic tension in the disclination line and show how the director configuration close to a +1/2 surface defect is influenced by the fact that the three elastic constants are different. A tilt is induced close to the surface that can be amplified and visualized by applying a voltage.

1. Introduction

Nematic liquid crystals (NLCs) are widely used in displays and optical components. The LC alignment can be homogeneous over the substrate, but also patterned photo-alignment has become an industrial alternative.[1] Recently there have been several reports on NLC devices with at least one substrate with patterned planar alignment.[1,2] The alignment direction may be a continuous function, but the pattern may also contain defect points in which the direction is not well-defined.[2a-c,3] A charge s (-1, -1/2, +1/2, +1, etc.) is typically attributed to defects

to indicate the rotation of the alignment direction when encircling the defect. Near a defect in the origin with charge *s*, the azimuthal angle of the alignment is given by $\varphi_0+s.\arctan(y/x)$. By imposing alignment defects at the surfaces, a rich variety of topological defects in the LC bulk can arise. Disclination lines appear in which the LC director is not well-defined, with a small radius (< 100 nm) in which the order parameter is reduced. Recently there has been a renewed interest in the theoretical treatment of disclination lines, describing their behaviour in the neighbourhood of defects and their dynamics.[4] Disclination lines provide a topological stability that can be instrumental for new switching modes, to realize bistable switching, etc. Studying the formation, interaction and responsiveness of LC disclinations is therefore not only interesting from a theoretical point of view but also opens up new possibilities for technological applications.

Disclination lines can connect defects defined at the surface or can form closed loops in the bulk of a NLC, for example when encircling colloidal inclusions,[5] or when rapid but continuous variations in the alignment direction occur independently at opposing substrates of a device.[1d,1e,1h,1i,3c] To realize patterned surface anchoring, scribing, micro-rubbing, surface topography, pillars and photo-alignment have been used.[1,2] In the case of strong anchoring, a defect in the alignment pattern with charge s generates 2|s| disclination lines in the bulk of the LC. In the case of weak anchoring and gliding, defects can become mobile and disclinations lines may connect two defects of the same charge on opposing substrates.[6] Thanks to photo-alignment, stable defects can now easily be realized experimentally, as has been demonstrated in a few papers.[1d,1e,3]

The flexibility of photo-alignment patterning in combination with the stimuli-responsiveness (e.g. electrical tunability) of LCs allows to design disclination networks with preprogrammed functionality.[2b,3c] Enhanced understanding of the LC behavior in cells with 2D patterns of topological defects is however still necessary to successfully engineer functional LC devices such as multistable photonic components, programmable origami or devices with directed

self-assembly of colloidal particles. To study the interaction of NLC disclination lines and their behavior under applied voltages, we defined a square grid pattern of ½ defects on the bottom substrate in combination with a uniformly planar aligned top substrate. Different types of interconnections occur between the +1/2 and -1/2 surface defects, and the three most common types of bulk disclinations are analyzed in detail by comparing experiments with numerical simulations (with and without applied voltage). In the discussion section also a theoretical analysis is provided, explaining the curvature of the different disclination lines and including the effect of unequal elastic constants for splay, twist and bend. To reduce the splay energy, a tilt of the director is induced close to the +1/2 surface defect. We managed to make this visible in the microscope by increasing the tilt under influence of an electric field .

2. Alignment configuration

We use the periodic photo-alignment pattern on the bottom substrate shown in **Figure 1**. The alignment pattern has period *P* in x and y directions and contains four half-integer defects in each unit cell, two +1/2 and two -1/2 defects, positioned on a square grid. This grid has two mirror symmetry planes perpendicular to the y-axis per unit cell (at y = 0 and at y = *P*/2), and four rotation centres of order 2 per unit cell (at x = ±*P*/4; y = ±*P*/4). These symmetry elements correspond to the wall-paper symmetry group p2mg (orbifold notation 22*). The alignment at the top substrate of the cell is uniform and approximately along the +x-direction, with a small pretilt (≈ 2°) towards the +z direction. In other words, the rubbing was along the –x direction as indicated in Figure 1.

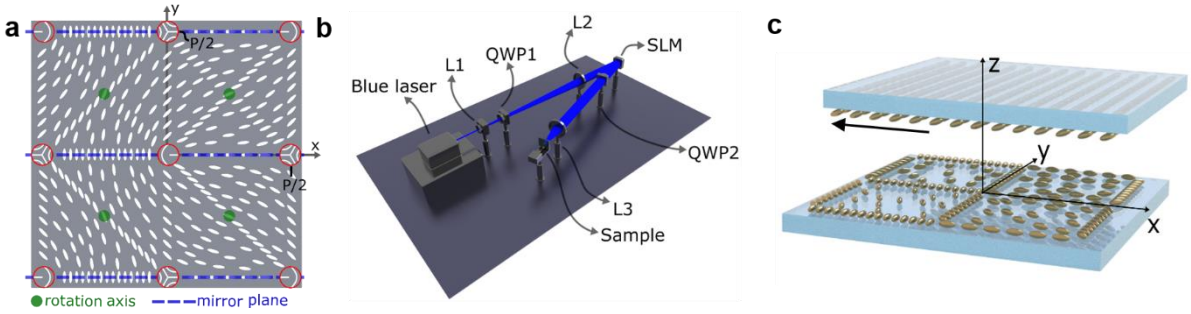

Figure 1. LC alignment pattern. a) Unit cell of the photo-alignment pattern of the director at the bottom substrate with period *P*, with indication of the +1/2 and -1/2 defects (red circles), symmetry planes (blue dashed lines) and two-fold rotation axes (green dots). b) Setup to create the alignment pattern with a blue laser, a spatial light modulator (SLM), three lenses and two quarter wave plates (QWPs). C) 3D image illustrating the alignment pattern at the bottom substrate and the rubbing direction (black arrow) and pretilt of the uniform planar alignment at the top substrate.

In the neighborhood of the +1/2 defect in the origin, the alignment is tangent to parabolas with focal point in the origin. In the neighborhood of the -1/2 defects, the alignment pattern has a rotation centre of order 3. The alignment in the rest of the unit cell with $|x| < P/2$ and $|y| < P/2$ is defined by the angle φ between the x-axis and the preferred alignment direction, inspired by the work of Murray et al. [2a]:

$$\varphi(x,y) = \frac{1}{2}\arctan\frac{y.(P-2|y|)}{x.(P-2|x|)}$$

The rubbing boundary condition (including pretilt) at the top surface (φ = 0°) maintains the mirror symmetry of the bottom substrate with respect to the y = 0 and y = *P*/2 planes. However, the rotation symmetry of order two for the bottom substrate is lost due to the pretilt.

3. Results

3.1. Microscopy

Devices with the outlined periodic photo-alignment pattern at the bottom substrate with *P* = 40 µm and planar rubbing at the top substrate are filled with the liquid crystal E7 (Δn=0.2, *d* = 5.5 µm) and observed under the microscope, with and without polarizers (see Methods). In **Figure 2** disclination lines appear as dark lines that connect a +1/2 defect with a -1/2 defect, both on the bottom surface. Usually the connected defects are nearest neighbors, but disclination lines may also connect defects that are further away as illustrated by the S-shaped disclination line in Figure 2f. We will focus on the analysis of disclination lines that are connecting nearest neighbors. These come into different shapes: horizontal (along x) and

vertical (along y) disclination lines, and may have different curvature. Shorter disclination lines (with less curvature) are usually more abundant than longer disclination lines.

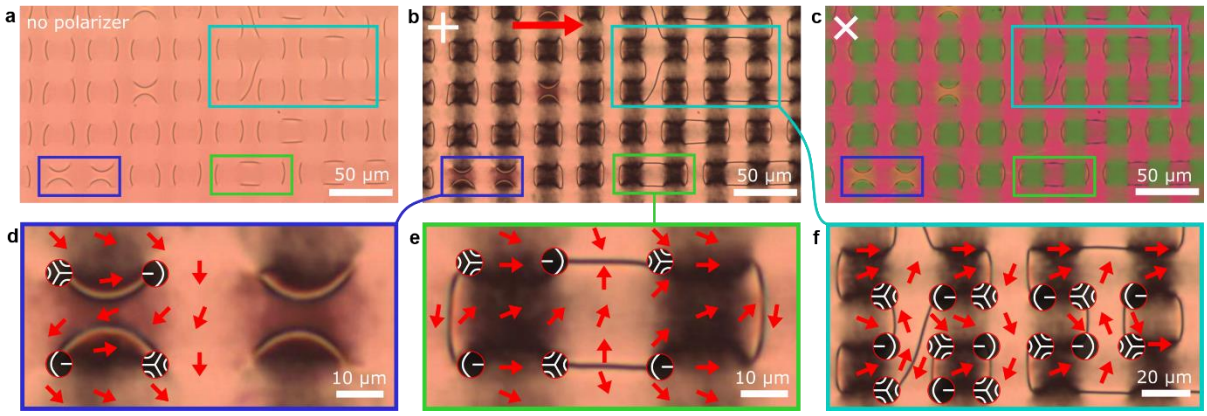

Figure 2. Polarization microscope images. a,b,c) overview images, without polarizers (a), with crossed polarizers horizontal and vertical (b), with crossed polarizers under 45° (c). d,e,f) details of (b) indicating the four types of defects, with the azimuth angle φ at the bottom substrate indicated by a red arrow: four strongly curved horizontal disclination lines (d); two horizontal and two vertical disclination lines (e); different kinds of disclination lines (f). The red arrows illustrate the director, near the top surface due to rubbing (b) and near the bottom surface due to photoalignment (d,e,f).

Figure 3 shows how the microscope images change over time when a sinusoidal potential difference of 1.5 V_{rms} (Volt root mean square) is applied between the two homogeneous electrodes at the top and bottom substrates (supporting information, video S1). Around the +1/2 defects with φ = 0° on their right, a domain becomes visible and disappears after a few seconds. The pattern of disclination lines is typically formed during cooling down from the isotropic phase and is not modified by the application of a small voltage. When higher voltages are applied it is possible to modify the disclination line configuration, favoring vertical interconnections along y (see supporting information, video S2). Executing a pressure on the substrates causes a flow in the LC, which may drag the disclination lines along. Disclination lines that touch each other may exchange their ends, which leads to a modified interconnection pattern. Typically a flow in the x-direction can lead to a larger number of horizontal disclination lines (see supporting information, video S3).

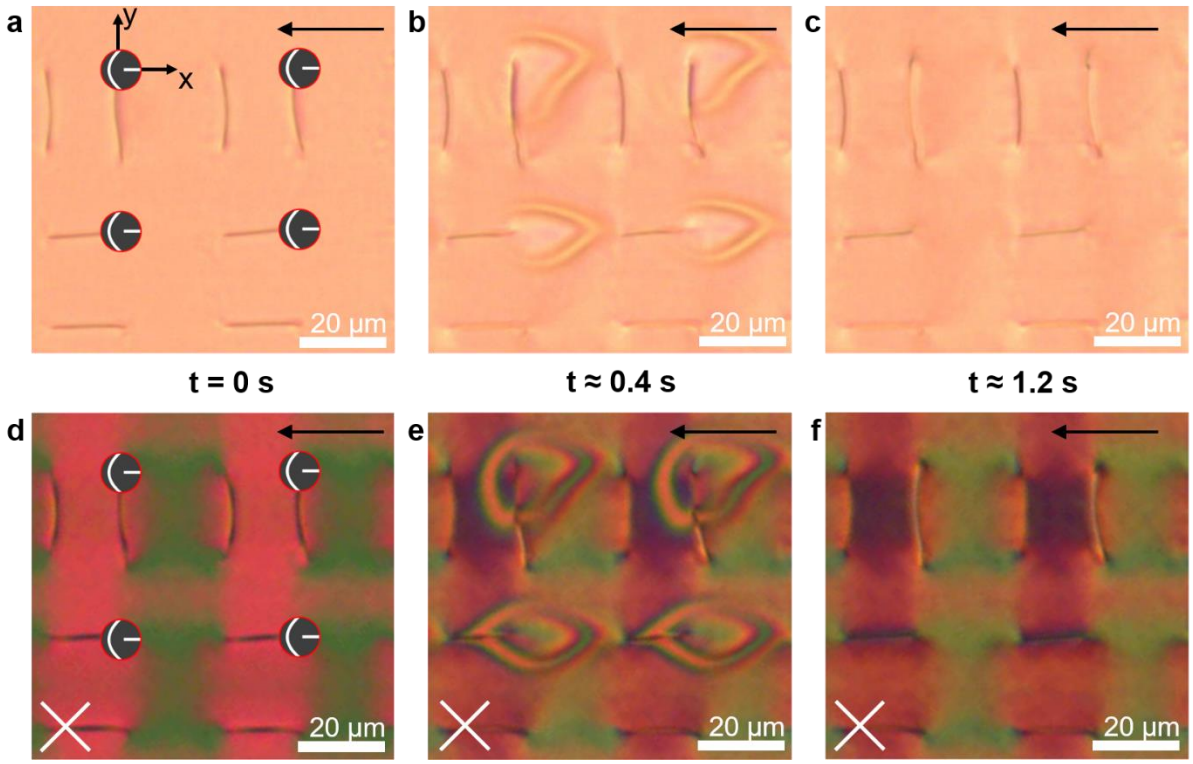

Figure 3. Polarization microscope images after application of a voltage. a,b,c) Microscope images at t ≈ 0, 0.4 and 1.2 s after switching to 1.5 V_{rms} , without polarizers. d,e,f) Microscope images at t ≈ 0, 0.4 s and 1.2 s after switching 1.5 V_{rms}, with crossed polarizers. In b and e domain walls are visible around the +1/2 defects with alignment in the +x direction. The rubbing direction at the top substrate is indicated with a black arrow.

3.2. Numerical simulations

Numerical simulations of the director distribution and the optical transmission have been carried out for a *P x P x d* unit cell based on the Q-tensor formalism and a beam propagation method (see Methods) for a device with the described alignment with P = 40 µm and d = 5.5 µm. **Figure 4** shows for each of the three types of disclination lines the orientation of the mid-plane director (z = 2.75 µm), the orientation of the director in a vertical section (variable z) through the middle of the disclination line, and the optical transmission for two orientations of the polarizers. In the transmission images the disclination lines appear as narrow dark lines. The disclination lines remain just below the mid-plane (z < d/2).

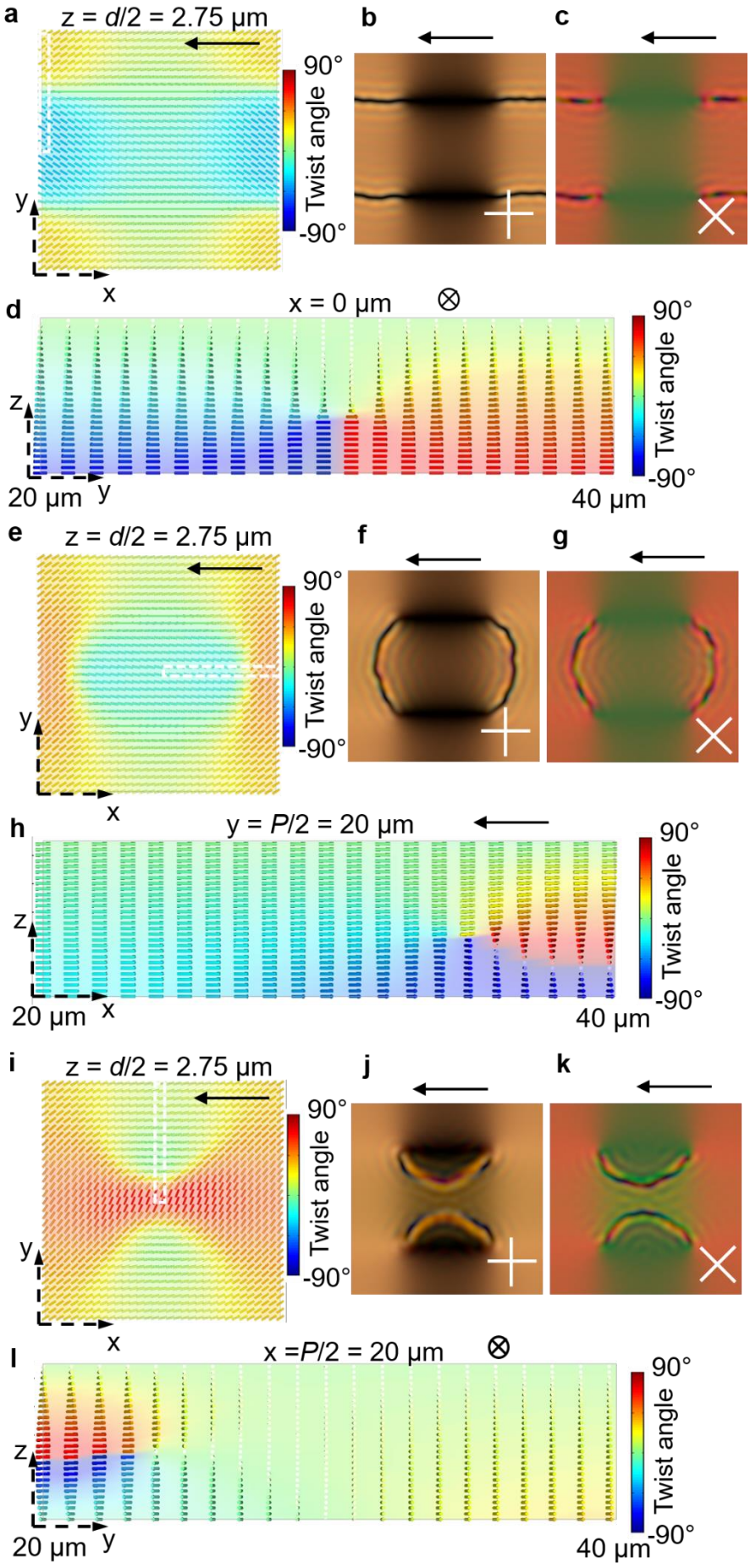
a
z = d/2 = 2.75 μm
90°
Twist angle
-90°
y
x
b
c
d
x = 0 μm
z
20 μm
y
40 μm
e
z = d/2 = 2.75 μm
f
g
h
y = P/2 = 20 μm
i
z = d/2 = 2.75 μm
j
k
l
x =P/2 = 20 μm

Figure 4. Numerical simulation of the LC director and light transmission for three types of disclinations without applied voltage. a,b,c,d) horizontal disclinations; e,f,g,h) vertical disclinations; i,j,k,l) curved horizontal disclinations. Director distribution in the mid-plane (a,e,i) with color indicating twist; transmission for 0/90 polarizers (b,f,j); transmission for +45/-45 polarizers (c,g,k); director distribution in a cross-section in the middle of the disclination lines (d,h,l) with color indicating twist. The rubbing direction at the top substrate is indicated with a black arrow.

Figure 5 and figure 6 show the simulated director distribution and optical transmission when a pulse of 1.5 V_{rms} has been applied over the electrodes, during switching. Figure 5 and 6 respectively show the results for curved vertical disclination lines and horizontal disclination lines. This illustrates that a domain is created around one of the +1/2 defects in which the director tilts in the opposite direction than in the rest of the cell. This domain disappears in the steady state configuration, after the voltage has been on for a long time.

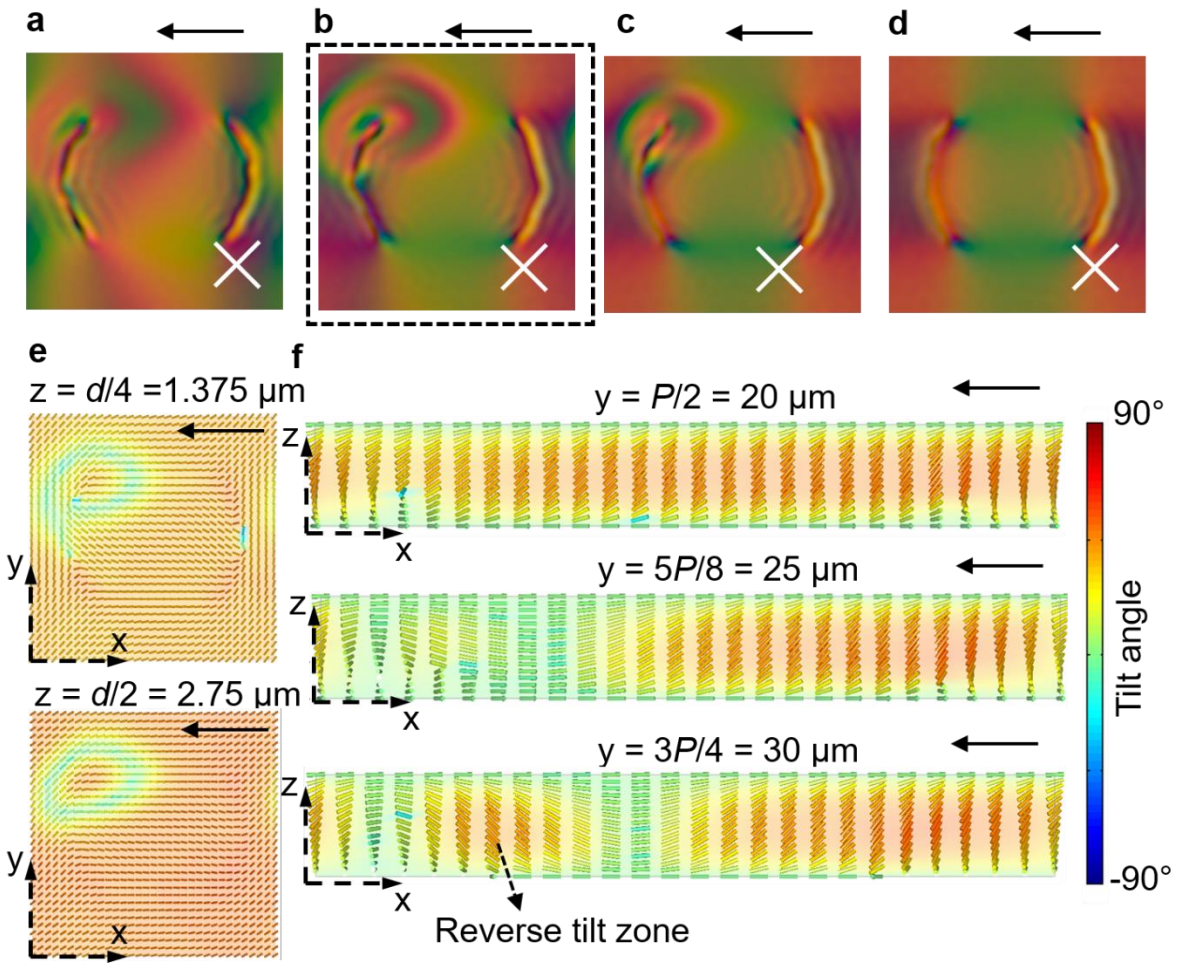

Figure 5. Numerical simulation of the LC director and light transmission during switching, after applying a voltage of 1.5 V_{rms} to a grid of curved vertical disclination lines. a-d)

Simulated transmission for +45/-45 polarizers (time after applying 1.5 V_{rms} is increasing from (a) to (d)). e) Director distribution for different sections at constant height z (colour indicates tilt) for case (b). f) Director distribution for different cross-sections of the disclination lines with constant y position (colour indicates tilt) for case (b). The rubbing direction at the top substrate is indicated with a black arrow.

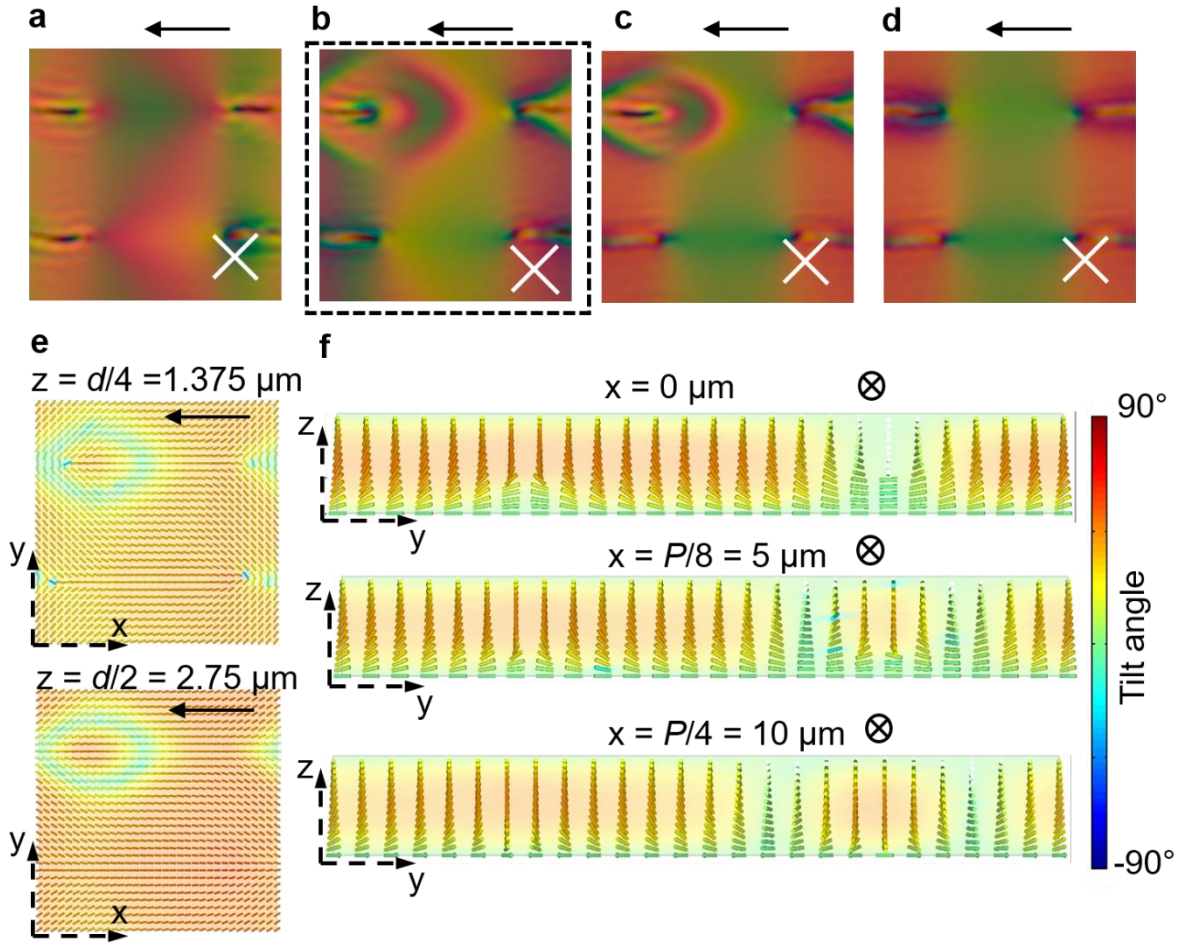

Figure 6. Numerical simulation of the LC director and light transmission during switching, after applying a voltage of 1.5 V_{rms} to a grid of horizontal disclination lines. a-d) Simulated transmission for +45/-45 polarizers (time after applying 1.5 V_{rms} is increasing from (a) to (d)). e) Director distribution for different sections at constant height z (colour indicates tilt) for case (b). f) Director distribution for different cross-sections of the disclination lines with constant x position (colour indicates tilt) for case (b). The rubbing direction at the top substrate is indicated with a black arrow.

3.3. Discussion

The comparison between Figure 2-3 and Figure 4-6 indicates a good correspondence between experimental microscope images and numerically simulated graphs. This confirms that the simulated director configurations that are outlined in Figure 4-6 are good approximations of the actual behavior. Figure 4 indicates that, when no voltage is applied, the director stays more or less parallel to the substrates (low tilt) in the entire volume and that the most

important elastic deformation is twist. If we do not consider the regions near the disclination lines, then the director variation is mainly a continuous twist from azimuth zero at the top substrate to an azimuth $\Phi(x,y)$ at the bottom surface, as illustrated by the red arrows in Figure 2. Note that the twist $\Phi(x,y)$ may differ by $\pm\pi$ from the azimuth angle $\varphi(x,y)$ that is defined by equation 1. In the region on the x-axis with $0 < x < P/2$ the photo-alignment is parallel to the x-axis ($\varphi = 0$) and the twist is typically zero ($\Phi = 0$). The twist $\Phi(x,y)$ varies continuously over the surface, with discontinuities of magnitude π between both sides of a disclination line (**Figure 7**).

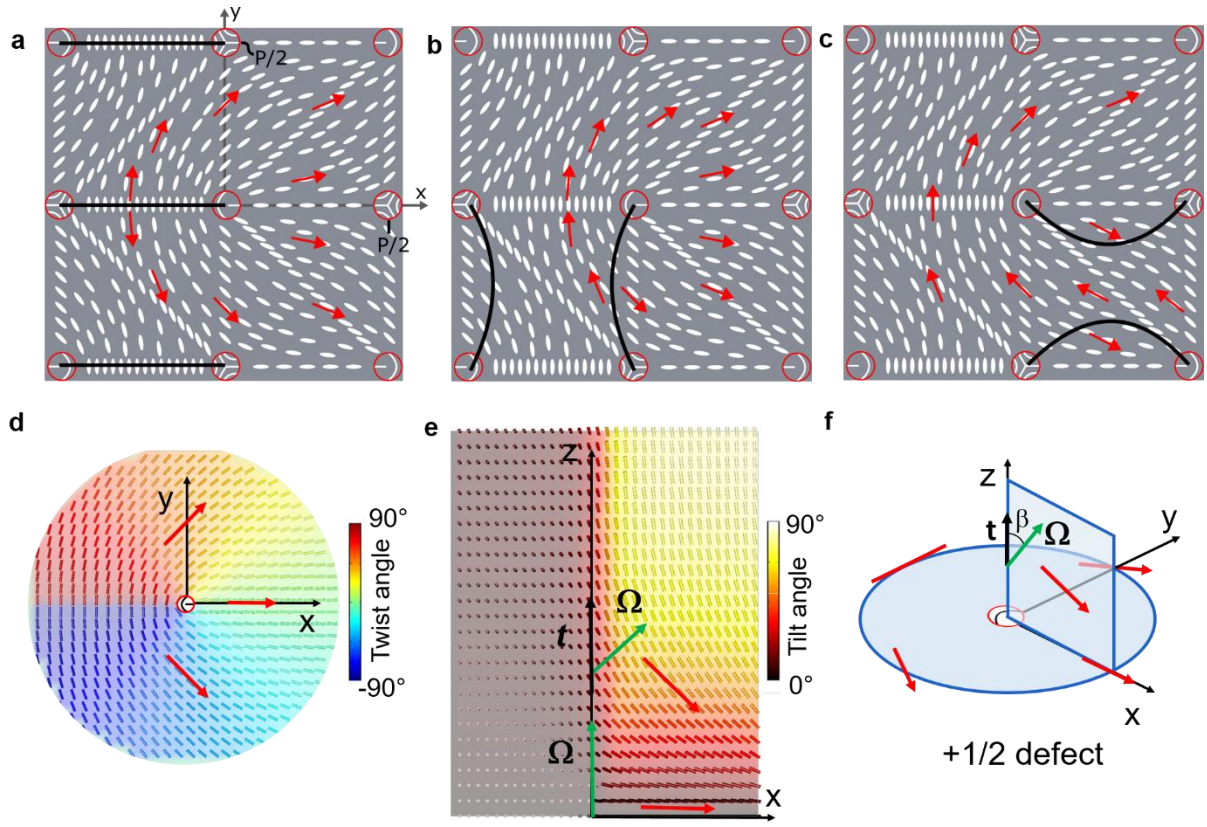

Figure 7. Disclination line properties. Schematic overview of three types of disclination lines: a) horizontal disclinations; b) vertical disclinations with curvature; c) horizontal disclinations with curvature. The red arrow indicates the azimuth Φ. Simulation of a small region near the +1/2 defect: d) alignment at the bottom electrode (color indicates twist); e) xz section of the simulation result near the disclination (y = 0, color for tilt angle) with indication of the tangential vector **t** and rotation vector **Ω**; f) Schematic 3D figure with indication of the director near the defect.

To indicate the effect of unequal elastic constants, Figure 7d-e show the simulated director distribution for an area where a disclination line leaves a +1/2 defect. The simulation is carried out with strong anchoring at the bottom substrate and free anchoring at the sides and at the top of a cylindrical volume. The defect core is fixed along the z-axis. The twist disclination has lower energy than the wedge disclination, because K_{22} is the smallest elastic constant. Therefore the director above the x-axis tilts into the xz-plane, transforming the disclination from a wedge type at the surface towards a splay type disclination in the bulk.

We note in Figures 2 and 4 that there are three types of disclination lines between nearest neighbors with different curvature, as was also mentioned by Guo et al. [3c]. The three types are schematically indicated in Figure 7: a straight horizontal line above regions with $\varphi = \pm 90^{o}$; a curved vertical line above regions with $\varphi \approx \pm 45^{o}$; a strongly curved horizontal line near regions with $\varphi \approx 0^{o}$. The curvature of the disclination line can be related to the difference in energy density between regions at opposite sides of the disclination line. As twist is the most important deformation, the elastic energy per unit area can be approximated by $K_{22}\Phi^2 / 2d$ (except in the vicinity of the disclination lines). For the straight horizontal disclination lines the elastic energy per unit area at both sides ($\Phi = \pm 90^{o}$) of the disclinaton line is the same. For the other two kinds of disclination lines, the twist $|\Phi|$ and the energy density per unit area are different at both sides of the disclination line which leads to a force on the disclination line and induces its curvature. With *H* the energy per unit length of the twist disclination, the minimization of the total energy leads to a proportionality between the curvature $1/R$ and the difference in twist energy at both sides of the disclination line (see Supplementary Information):

$$\frac{H}{R} = \frac{K_{22}}{2d}\left(\Phi_1^2 - \Phi_2^2\right),$$

with Φ_1 and Φ_2 the total twist at both sides of the disclination line. For the vertical disclination lines the twist $|\Phi|$ at both sides can be approximated by respectively 135° and 45°, and we find the following expression for the radius of curvature: $R \approx 4Hd/(\pi^2 K_{22})$. We can estimate the radius in Figure 2e to be about 20 μm, which, together with d = 5.5 μm and K_{22} = 6.5 pN, yields H ~ 60 pN. This approach also explains why the longer S-shaped disclination line in Figure 2f has a variable curvature that becomes zero where it crosses the region with alignment along the y-axis ($\Phi = \pm 90°$).

For the theoretical discussion of the disclination lines itself, we introduce the tangent unit vector ***t*** along the disclination line, with the convention that it points towards the -1/2 surface defect.[4c,7] When encircling the disclination line in the direction according to the tangent vector and the right-hand rule, the LC director ***L*** approximately describes a half circle on the unit sphere. This directed half circle is determined by the rotation vector **Ω**, which varies along the disclination line. In the bulk, -1/2 and +1/2 disclinations are topologically equivalent and can be continuously transformed into one another. In the +1/2 surface defects the disclination is of the wedge type and according to the above definitions, **Ω** is parallel to **t**. In the -1/2 defects, the disclination is also of the wedge type, but with **Ω** antiparallel to **t**. In the central section of the disclination line, **Ω** is perpendicular to **t** and the disclination line is mainly of the twist type.

To get more insight in the director configuration and better understand the peculiar electrical switching behavior (Figure 3, 5 and 6), we theoretically investigate the characteristics of the disclination line close to a surface defect. In the theoretical treatment of disclination lines, the splay, twist and bend elastic constants are often chosen to be equal to each other (alternatively K_{22} is sometimes chosen differently).[1e, 4a,4c,5d] Based on that approximation, the director describes a uniform rotation, when the disclination line is encircled. To investigate the energy contributions of splay, twist and bend separately, we here use a different approximation, by

estimating the energy per unit length of the disclination line F_{discl} under the assumption that the director rotates uniformly on a large circle around the vector **Ω**. By integrating the elastic energy between the radius of the core r_{core} and a radius r_{max} corresponding to the geometry, we find the following expression (supporting information):

$$F_{discl} = \frac{\pi}{16}\left(K_{11}\left(1+\cos^2\beta\right)+2K_{22}\sin^2\beta+K_{33}\left(1+\cos^2\beta\right)\right)\ln\frac{r_{\max}}{r_{core}}+F_{core},$$

with β the angle between the tangent line **t** and the vector **Ω** (Figure 7f). The term between brackets varies between $2K_{11}+2K_{33}$ for a wedge disclination (β = 0 or π) and $K_{11}+2K_{22}+K_{33}$ for a twist disclination (β = π/2). Neglecting the energy in the core, we can estimate the energy per unit length for a twist disclination in E7: $8\ \mathrm{pN}\ln\left(r_{\max}/r_{core}\right)\sim 42\ \mathrm{pN}$ when the radius of the core and the radius of the surroundings are set for example to values of 10 nm and 2 μm respectively. This value is roughly of the same order as the value for *H* determined above. The energy minimization for the disclination line (see S2) leads to an approximate proportionality between the radius *R* and the thickness *d* of the device (assuming that *H* is independent from *d*), which means that we expect less curvature for a disclination line in a cell with larger thickness.

The variation in energy density with the angle β indicates that the vector **Ω** prefers to orient perpendicular to the tangential vector **t**. Near the +1/2 defect in the origin for $y = 0$ and $x > 0$, the derivative $\partial L_y/\partial y$ is positive (see Figure 1a). This means that the splay elastic energy can be lowered for a deformation $\partial L_z/\partial z < 0$ which leads to a torque in the +y direction.[8] Such a reorientation is indeed observed in the simulation of Figure 7d, for a cylinder with strong +1/2 defect alignment at the bottom surface and free alignment at all other surfaces. The typical variation of **Ω** is illustrated in the scheme of Figure 7e.

Usually it is not easy to directly obtain information about the director variation in the vicinity of a disclination line experimentally. However, by the application of an ac voltage over the

cell we are able to amplify the small tilt close to a +1/2 surface defect and make it visible in polarization microscopy. This is because the initial tilt near the disclination in the origin (Figure 7f) is opposite to the tilt defined by the rubbed top substrate (Figure 1c). As a result, when a voltage is applied, a domain wall is created around the defect in the origin. This is clearly visible in the microscope images (Figure 3b,3e). Over time the domain wall is moving towards the defect and finally the tilt near the defect is reversed (Figure 3c and 3f). For the disclination line that starts in the +1/2 defect positioned at (P/2,P/2,0), the tilt is in the same direction as for the top surface and no reverse tilt zone is observed when applying a voltage. Note that the reverse tilt can be observed for both horizontal and vertical disclinations (Figure 3f). The reverse tilt zone is also observed in the numerical simulations (Figure 5 and 6) that are obtained during switching when applying 1.5 V_{rms}. The region with reverse tilt is limited by a complex surface that is bound by a spiral at the bottom surface and by the disclination line, as can be seen in Figure 5e,f and Figure 6 e,f. This domain disappears when converging towards the steady state situation Figure 5d,6d.

The phase retardation $\Gamma=2\pi\Delta nd/\lambda$ in the liquid crystal layer we consider here is much larger than the twist angle Φ, which means that light transmission can be described by the Mauguin regime. This implies that for an x-polarized plane wave that enters from the top substrate, the polarization plane is rotated over an angle Φ and leaves the bottom substrate with polarization according to the director distribution shown in Fig.1a. This allows to explain the transmission distribution for crossed polarizers in Fig.4b and 4f: low transmission where $\Phi = 0^o$ and high transmission where $\Phi = 90^o$. The diffraction pattern for the stabilized periodic structures will as well depend on the disclination interconnection and the applied voltage. If the disclination line is according to Fig. 4a, the zero diffraction order will be purely polarized along x, because the xz plane is a symmetry plane of the structure. If on the other hand the disclination line is according to Fig. 4e, then the zero diffraction order will be mainly polarized along y. This

illustrates that different disclination interconnections based on the alignment according to Fig.1a lead to very different diffraction patterns. When appropriate electrodes and waveforms can be found to realize switching between multistable interconnecting states, it should be possible to realize switchable diffraction gratings.

4. Conclusion

We have realized LC devices with disclination grids based on a periodic array of +1/2 and -1/2 defects obtained by photo-alignment at the bottom substrate and homogeneous rubbing at the top substrate. This leads to a non-periodic network of different kinds of disclination lines. The director configuration and disclination lines are identified by numerical simulations and polarization microscopy images. The curvature of a disclination line could be linked to the difference in twist energy at both sides of the disclination line. We have also shown that the +1/2 defect induces a region with a preferred pretilt to reduce the splay energy, by taking into account the difference in elastic energy constants for splay, twist and bend. The pattern around a +1/2 defect determines the tilt direction during switching under influence of a voltage. The observed switching behavior, with the temporary appearance of a domain with reverse tilt, is fully explained by the theoretical and numerical investigation. In general, the obtained results indicate that LC defect grids with small dimensions may be understood if a sufficient level of detail is used in the analysis. By reducing the dimensions of these defect grids further, these devices may be used as switchable scattering centres. The pattern of disclination interconnections is relatively stable and may be used to encode information. The switching with a voltage may be used in smart windows.

5. Methods

Device design: The devices use cleaned square one-inch glass substrates that are coated with the transparent electrode ITO. The bottom substrate is treated with ozon-plasma after which

the photo-alignment solution is spin-coated (3000 rpm, 30 s). The photo-alignment material is brilliant yellow (Sigma-Aldrich, 0.2 wt%) and is solved in dimethylformamide (Sigma-Aldrich). After spin-coating, the sample is placed on a hotplate at 90 °C for 5 minutes. Brilliant yellow can be oriented by illumination with linearly polarized (UV or) blue light, resulting in a LC alignment that is perpendicular to the orientation of the linear polarization. Non-uniform LC alignment can be obtained with the help of patterned illumination. The desired alignment pattern on the substrate is translated into a retardation matrix for the pixels of the spatial light modulator (SLM) that is used for the illumination procedure. The SLM (Holoeye Pluto 2) that is used has a resolution of 1920 by 1080 pixels and a pixel pitch of 8 μm. Using a projection lens, the pattern displayed on the SLM is scaled down by a factor of 11.6. The beam of a blue laser (Cobolt Twist, wavelength 457 nm, 200 mW) is first transformed into circularly polarized light and then reflected by the SLM with a phase delay between the vertical and the horizontal field components (Figure 1b). The phase delay determines the azimuthal angle of the linearly polarized light that is incident onto the sample.[1d] The period *P* of the pattern is chosen to be 40 μm.

The top substrate is covered with a homogeneously rubbed nylon thin film. The rubbing cloth is moved in the -x direction with respect to the top substrate, which leads to a preferred alignment parallel to the +x-axis, with a small pretilt towards the +z axis. The two substrates are glued together, using a UV curable glue (NOA68) at the edges of the substrates that contains spacers with diameter 5.5 μm. The empty space is then filled with the LC E7 at 80^{o}C, above the clearing temperature.

Numerical simulations: The simulation of the director configuration follows from a minimization of the total energy in a unit cell, being the sum of elastic distortion energy, thermotropic (or Landau) energy, electrical energy and surface energy.[9] The LC is at each point in the volume characterized by a Q-tensor and the energy terms can be expressed as a

function of Q and its spatial derivatives using the conventional parameters for E7 (K_{11} = 11.1 pN, K_{22} = 6.5 pN, K_{33} = 17.1 pN, ε_{perp} = 5.2, ε_{para} = 19, A = -174 N/m^2, B = -2120 N/m^2, C = 1740 N/m^2).[1d,10] At the top and bottom boundaries we assume strong anchoring with a pretilt of 2^o at the rubbed interface and zero pretilt for the bottom substrate, with azimuthal anchoring defined by Equation 1. Periodic boundary conditions are applied for the interfaces at $|x| = P/2$ and $|y| = P/2$. A tetrahedral mesh is used to describe the volume of the LC and a voltage can be applied between the z = 0 and z = *d* coordinate. The numerical solutions in the volume contain disclination lines and the mesh is sufficiently small to ensure the mobility of the disclination lines during the optimization process.

The numerical simulation of the transmission for crossed polarizers is made by the open-source software Nemaktis that is based on a generalized beam propagation method.[11] The incident light is linearly polarized, and after transmission through the LC layer the light passes through a second polarizer.

Supporting Information

Supporting Information is available from the Wiley Online Library or from the author.

Acknowledgements

We would like to acknowledge Miha Ravnik for interesting discussions on the numerical simulations.

This work has been made possible by funding by the Flemish fund for scientific research under grant number FWOOPR2021008601.

Brecht Berteloot is being sponsored by a Baekeland mandate of VLAIO.

Received: ((will be filled in by the editorial staff))
Revised: ((will be filled in by the editorial staff))
Published online: ((will be filled in by the editorial staff))

References

[1] a) O.Yaroshchuk, Y. Reznikov, *J. Mater. Chem.* **2012**, *22*, 286; b) J. Kim, M.J. Escuti, *J Opt Soc Am B.* **2019**, *36(5)*, D42-D46; c) T. Zhan, J. Xiong, G. Tan, Y.-H. Lee, J. Yang, S. Liu, S.-T. Wu, *Opt. Express* **2019**, *27*(11), 15327-15334; d) B. Berteloot, I. Nys, G. Poy, J.

Beeckman, K. Neyts, *Soft Matter* **2020**, *16*(21), 4999-5008; e) M. Wang, Y. Li, H. Yokoyama, *Nat. Commun* **2017**, *8*, 388; f) I. Nys, V. Nersesyan, J. Beeckman, K. Neyts, *Soft Matter* **2018**, *14*(33), 6892-6902; g) J. Kobashi, H. Yoshida, M. Ozaki, *Nat. Photon*. **2016**, *10*, 389-392; h) I. Nys, *Liquid Crystals Today* **2020**, *29*(4), 65-83; i) K. Sunami, K. Imamura, T. Ouchi, H. Yoshida, M. Ozaki, *Phys. Rev. E.* **2018**, *97*, 020701.

[2] a) B. S. Murray, R. A. Pelcovits, C. Rosenblatt, *Phys. Rev. E.* **2014**, *90*, 052501; b) S. Harkai, B. S. Murray, C. Rosenblatt, S. Kralj, *Phys. Rev. Research.* **2020**, *2*, 013176; c) J. Fleury, D. Pires, Y. Galerne, *Phys. Rev. Lett.* **2009**, *103(26)*, 267801; d) M. Honma, T. Nose, *Jpn. J. Appl. Phys.* **2003**, *42*, 6992-6997; e) M. Kim, F. Serra, *Crystals* **2020**, *10*(4), 314; f) I. Nys, K. Chen, J. Beeckman, K. Neyts, *Adv. Opt. Mater.* **2018**, *6*, 1701163; g) I. Nys, J. Beeckman, K. Neyts, *Adv. Opt. Mater.* **2018**, *6, 1800070;* h) I. Nys, J. Beeckman, K. Neyts, *Opt. Express* **2019**, *27*(8), 11492-11502; i) S. P. Palto, A. R. Geivandov, I. V. Kasyanova, V. V. Artemov, and M. V. Gorkunov, *JETP Lett.* **2017**, *105*, 174–178.

[3] a) B. Berteloot, I. Nys, X. Xue, J. Beeckman, K. Neyts, *Journal Mol. Liq.* **2021**, *337*, 116238; b) H. Yoshida, K. Asakura, J. Fukuda, M. Ozaki, *Nat. Commun*. **2015**, *6*, 7180; c) Y. Guo, M. Jiang, S. Afghah, C. Peng, R. L. B. Selinger, O. D. Lavrentovich, Q.-H. Wei, *Adv. Opt. Mater.* **2021**, 2100181; d) C. Peng, Y. Guo, T Turiv, M. Jiang, Q.-H. Wei , O. D. Lavrentovich, *Adv. Mater.* **2017**, 1606112.

[4] a) S. Copar, S. Zumer, *P Roy Soc a-Math Phy.* **2013**, *469*, 2156; b) X. Yao, H. Zhang, J. Z. Y. Chen, *Phys. Rev. E.* **2018**, *97*, 052707 ;c) C. Long, X. Tang, R. L. B. Selinger, J. V. Selinger, *Soft Matter*. **2021**, *17*, 2265-2278; d) G. Duclos, R. Adkins, D. Banerjee, M. S. E. Peterson, M. Varghese, I. Kolvin, A. Baskaran, R. A. Pelcovits, T. R. Powers, A. Baskaran, F. Toschi, M. F. Hagan, S. J. Streichan, V. Vitelli, D. A. Beller, Z. Dogic, *Science.* **2020**, *367(6482)*, 1120-1124.

[5] a) A. Martinez, M. Ravnik, B. Lucero, R. Visvanathan, S. Žumer,

I. I. Smalyukh, *Nat. Mater.* **2014**, *13*, 258; b) U. Tkalec, M. Ravnik, S. Čopar, S. Žumer, I. Muševič, *Science* **2011**, 333, 62-65; c) L. Tran, M. O. Lavrentovich, D. A. Beller, N. Li, K. J. Stebe, R. D. Kamien, *PNAS.* **2016**, *113,* 7106-7111; d) I. I. Smalyukh, B. I. Senyukh, S. V. Shiyanovskii, O. D. Lavrentovich, A. N. Kuzmin, A. V. Kachynski, P. N. Prasad, *Mol. Cryst. Liq. Cryst.* **2006**, *450*, 279-295.

[6] K. Harth, R. Stannarius, Front. Phys. 2020, 8,112.

[7] P. G. de Gennes, J. Prost, *The Physics of Liquid Crystals*, Oxford University Press: Oxford, UK **1993**.

[8] E. C. Gartland, *Continuum Mech. Therm.* **2020**, *32*(6), 1559-1593.

[9] a) R. James, E. Willman, F. A. Fernández, S. E. Day, *IEEE Trans. Electron Devices* **2006**, *53*, 1575; b) E. Willman, F. A. Fernández, R. James, S. E. Day, *J. Disp. Technol.* **2008**, *4*, 276.

[10] a) I. Nys, J. Beeckman, K. Neyts, *Soft Matter* **2015**, *11*(39), 7802-7808; b) I. Nys, B. Berteloot, G. Poy, *Crystals* **2020**, *10*(9), 840.

[11] a) G. Poy, S. Zumer, *Opt Express* **2020**, *28(*16), 24327-24342.

The table of contents entry should be 50–60 words long and should be written in the present tense. The text should be different from the abstract text.

I.Nys, B. Berteloot, J. Beeckman, K. Neyts*

Nematic liquid crystal disclination lines driven by a photo-aligned defect grid

ToC figure ((Please choose one size: 55 mm broad × 50 mm high **or** 110 mm broad × 20 mm high. Please do not use any other dimensions))

Supporting Information

Nematic liquid crystal disclination lines driven by a photo-aligned defect grid

*Inge Nys, Brecht Berteloot, Jeroen Beeckman and Kristiaan Neyts**

S1 Estimation of the energy in a disclination line, assuming three different elastic constants.

The elastic energy density by Oseen and Frank, as a function of the director L is given by:

$$F = \frac{1}{2}K_{11}\left(\nabla\cdot\bar{L}\right)^2 + \frac{1}{2}K_{22}\left(\bar{L}\cdot\nabla\times\bar{L}\right)^2 + \frac{1}{2}K_{33}\left(\bar{L}\times\nabla\times\bar{L}\right)^2$$

Working in cylinder coordinates (r,φ,z), and neglecting a z-dependency (because we align the z-axis along the disclination line) we obtain:

$$F = \frac{1}{2}K_{11}\left(\frac{1}{r}L_r + \frac{1}{r}\frac{\partial L_\varphi}{\partial\varphi}\right)^2 + \frac{1}{2}K_{22}\left(L_r\frac{1}{r}\frac{\partial L_z}{\partial\varphi} + \frac{L_z}{r}L_\varphi - \frac{L_z}{r}\frac{\partial L_r}{\partial\varphi}\right)^2 + \frac{1}{2}K_{33}\left(\left(\frac{1}{r}L_\varphi L_\varphi - \frac{1}{r}L_\varphi\frac{\partial L_r}{\partial\varphi}\right)^2 + \left(\frac{1}{r}L_z\frac{\partial L_z}{\partial\varphi} - \frac{1}{r}L_r L_\varphi + \frac{1}{r}L_r\frac{\partial L_r}{\partial\varphi}\right)^2 + \left(-\frac{1}{r}L_\varphi\frac{\partial L_z}{\partial\varphi}\right)^2\right).$$

We assume that the director rotates around the rotation vector with inclination angle θ_R. In this case the director is given by:

$$\bar{L} = \left(\cos\psi\cos\varphi\cos\theta_R + \sin\psi\sin\varphi\right)\bar{e}_r + \left(-\cos\psi\sin\varphi\cos\theta_R + \sin\psi\cos\varphi\right)\bar{e}_\varphi - \cos\psi\sin\theta_R\bar{e}_z$$

With ψ the azimuthal angle of the rotation around the rotation vector. In the case of a disclination line, the azimuthal angle increases by π when φ increases from 0 to π: $\psi = \varphi/2 + \psi_0$.

The resulting expression for *F* has many terms, but integration over a circle, with φ going from 0 to 2π while keeping r constant simplifies to:

$$\int_0^{2\pi} F\cdot r d\varphi = \frac{\pi}{16r}\left(K_{11}\left(1+\cos^2\theta_R\right) + 2K_{22}\sin^2\theta_R + K_{33}\left(1+\cos^2\theta_R\right)\right)$$

Integration between an inner radius r_{min} and an outer radius r_{max} leads to the elastic energy per unit length of the disclination line:

$$F_{disclination} = \frac{\pi}{16}\left(K_{11}\left(1+\cos^2\theta_R\right)+2K_{22}\sin^2\theta_R+K_{33}\left(1+\cos^2\theta_R\right)\right)\ln\frac{r_{\max}}{r_{\min}}$$

This approximation is an over-estimation, because the energy may further be reduced by allowing additional degrees of freedom in which the rotation of the director is not uniform when encircling the disclination line.

S2 Derivation of the curvature of a disclination line

The end points of the disclination line are fixed and separated by a distance P/2. The disclination line can be approximated by a circle with radius R and sector angle α. The total energy can be approximated by the sum of two terms.

- The energy in the disclination line (red) which is proportional with the length of the arc: αR
- The area of the circle segment (green) is given by:

$$\frac{R^2}{2}\left(\alpha-\sin\alpha\right)$$

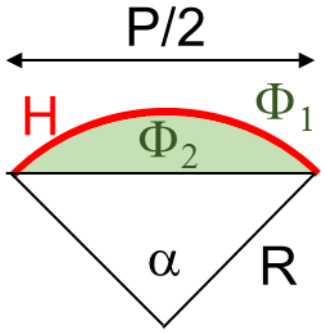

- The parameters R and α are linked by the expression for the length of the chord that should be equal to P/2:

$$\frac{P}{2} = 2R\sin\frac{\alpha}{2}$$

The total energy is given by:

$$\alpha RH + \frac{R^2}{2}\left(\alpha-\sin\alpha\right)\cdot\frac{K_{22}}{2d}\left(\Phi_2^2-\Phi_1^2\right)$$

with H the energy per unit length and $\frac{K_{22}}{2d}\Phi_1^2$ and $\frac{K_{22}}{2d}\Phi_2^2$ the elastic energy per unit area at both sides of the disclination line.

Minimization of the total energy with respect to R and α, taking into account the boundary condition between the two parameters, yields:

$$\frac{H}{R} = \frac{K_{22}}{2d}\left(\Phi_1^2 - \Phi_2^2\right)$$

Video S1. Movie of switching on the voltage of 1.5 V_{rms}, showing the reverse tilt zone near +1/2 defects (no polarizers are used in the microscope).

Video S2. Movie of switching on a high voltage of 7 V_{rms}, favoring vertical interconnections along y (no polarizers are used in the microscope).

Video S3. Movie showing the effect of an induced flow on the configuration of the disclination lines (crossed polarizers are used in the microscope).